Mars 2020 Center Differential Pivot Restraint: Flexurized Spring System Providing Compliance for Rover Mobility Deployment Prior to Landing

Matthew Cameron* and Kevin Liu*

Abstract

The Center Differential Pivot Restraint (CDPR) for the Mars 2020 mission is designed to constrain motion of the rover differential and to dampen out the load response during rover's mobility deployment event in Entry, Descent, and Landing (EDL) phase of the mission. For Mars 2020, it was required to redesign the mechanism to save minimum 33% of the mass from the previous Mars Science Laboratory (MSL) design. The new mechanism architecture used a monolithic spring-like flexure to act as the system compliance, resulting in 50% mass savings from the MSL design. Along the design and prototype testing process, several mechanism design principles were re-affirmed as well as lessons learned about potential race conditions.

Introduction

The Mars 2020 mission is designed to land and traverse a newly improved rover on Mars to gather soil samples that could be returned to Earth for detailed study. During the EDL portion of the mission, the rover is lowered from the sky crane via three bridle connections while the rover's mobility subsystem's rocker/bogie suspension on both sides of the rover deploys in preparation for surface touchdown (Fig. 1). During this deployment event, the CDPR absorbs and dampens out the induced load into the rover at the chassis top deck interface in the event when the side-to-side suspension deployment becomes asymmetric. Same as that of the MSL mission, the CDPR is mounted on the top deck of the rover chassis and located directly aft of the rover differential assembly (Fig. 2).

As improved upon the previous MSL CDPR [1], completely new design and architecture for the Mars 2020 CDPR were achieved by maintaining the same functionality, while reducing the restraint's mass by 50%. From conceiving the initial design in November 2015, through multiple design reviews and prototype testing, to completing flight integration and qualification testing around early January 2020, the entire cradle-to-grave process spanned over a 39-month period. This paper discusses details of the new Mars 2020 design and mechanism features, its development process, key improvements from the previous MSL mission, and the design validation testing campaign; highlighting key lessons learned throughout the design and testing process.

Mars 2020 vs. MSL Design

The design for Mars 2020 CDPR is composed of a spring-like flexure, constrained by a pyro pin-puller attached to the mobility differential on one end and a shoulder bolt to a bracket bolted to the rover chassis top deck on the other end (Fig. 2). Details of its design and the deployable mechanism are presented in a later section. For brevity and scope of this paper, see [1] for complete details of MSL's CDPR design.

In both designs, the mechanism's function is the same and is described in three phases: (1) rover mobility deployment response dampening and motion constrain during EDL, (2) CDPR mechanism deployment, and (3) remaining deployed for the remainder of surface operations. Major similarities of CDPR between the two missions include how each deployable is constrained to the differential as well as the main passive element in the deployment mechanism.

* Jet Propulsion Laboratory, California Institute of Technology, Pasadena, CA

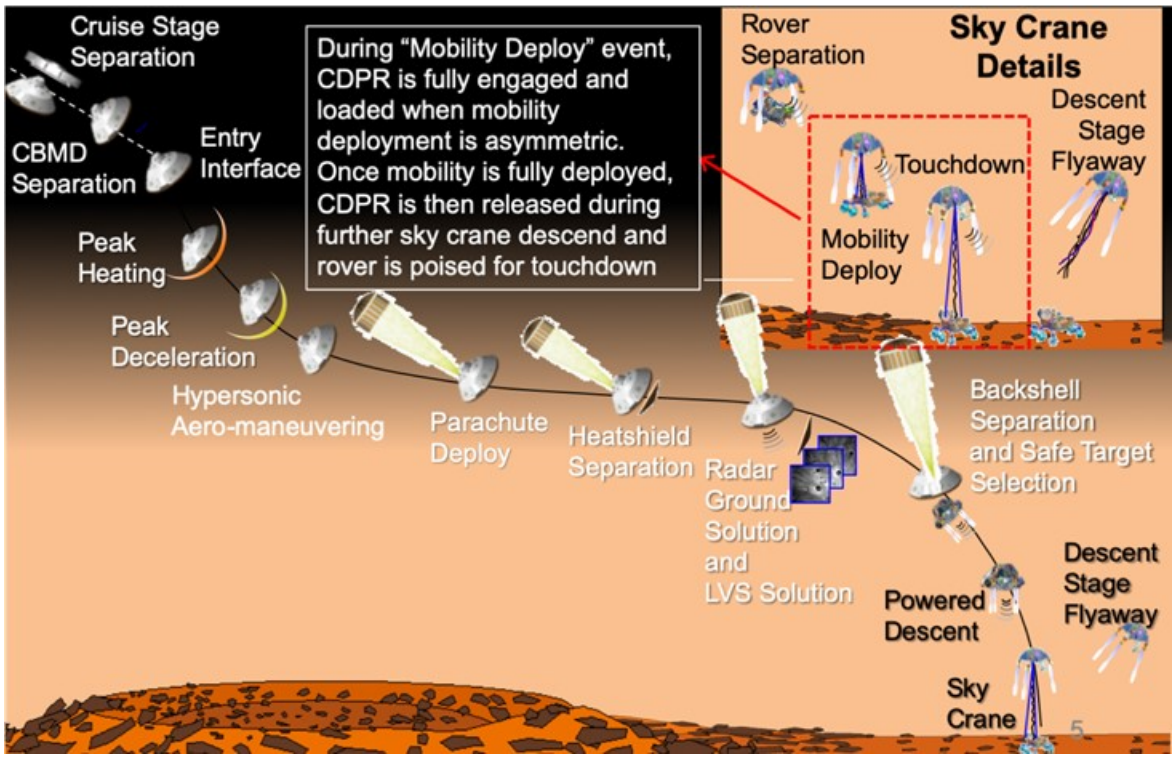

Figure 1. Mars 2020 EDL timeline indicating when the CDPR is actively engaged during the mobility deployment just prior to touchdown.

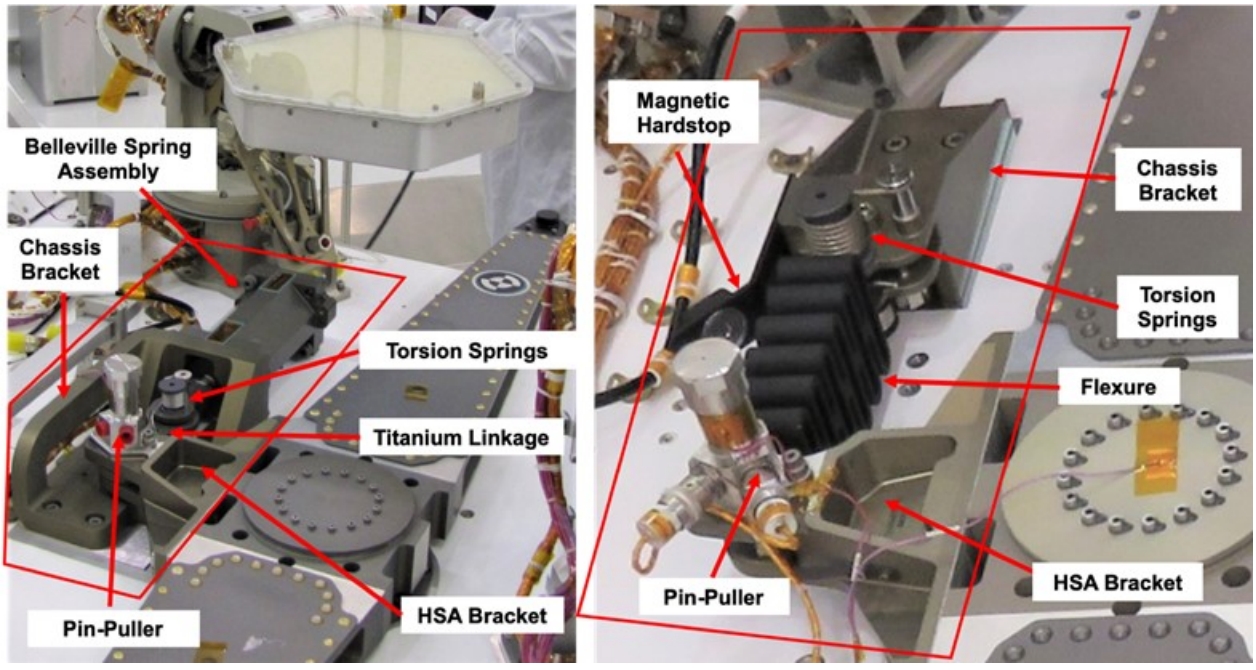

Figure 2: MSL CDPR (left) versus Mars 2020 CDPR (right)

The deployable for MSL and Mars 2020 are both constrained in place by a 9.5-mm (3/8-inch) diameter pin-puller pyro device. The pin-puller is in the same location relative to the Center Differential Pivot (CDP) and differential (Fig. 2). The MSL's CDPR dampened out the response from the asymmetric load using two mirrored stacks of belleville spring washers within a crank-slider mechanism [1]. A titanium linkage (weighing approximately 150 grams) coupled the pin-puller to the belleville spring washers. Immediately after the pin-puller was fired, only the titanium linkage was deployed and constrained in place by two torsion springs [1]. For Mars 2020, a steel spring-like flexure replaces the titanium linkage and the entire belleville spring assembly. Immediately after the pin-puller is fired, the steel flexure (weighing approximately 1500 grams) is deployed to a final stowed position and is also driven by two torsion springs. This is where the similarities between MSL and Mars 2020 CDPRs end.

Since the mass of the deployable for Mars 2020 was 10 times greater than that of MSL, a heavy emphasis on CDPR's ability to deploy its flexure and to ensure it remains deployed was put forth during the re-design process. As a result, this drove to four major mechanism design changes from MSL to Mars 2020. A summary of these changes are as follows:

- Size and strength increase of the torsion springs in order to achieve the required release torque
- Installment of a kickoff spring as a tertiary flexure release aid
- Installment of a magnetic latch into the deployable hard stop to further ensure the flexure to remain at a fully and final deployed position
- Having the spring element being between the spherical bearings ensured moment decouple or pure axial load transfer which eliminated alignment concerns that lead to several issues in the MSL's mechanism [1]

Details of the aforementioned mechanisms and structural features are discussed in later sections.

Lastly, even though the location of the CDPR relative to the differential was similar between MSL and Mars 2020, the mechanical interface between the rover chassis top deck had to be redeveloped. Part of what drove the MSL design was the shear pin interface between the CDPR and the top deck that not only required a time-consuming match drilling process but was also set by the time the compliant MSL CDPR had to be developed [1]. For the Mars 2020 design, this interface was renegotiated to avoid using match drilled shear pins and allowed for easier integration to the chassis top deck. Instead, a singular shear feature was created. The shear feature is a monolithic planar extrusion with a tightly toleranced diameter from the bottom of the chassis bracket that mated to a pocket on the rover chassis top deck. Along with the four bracket mounting fasteners, the designed size and fitment tolerance of the shear boss were intended to take the entire shear load through the CDPR if the frictional capability of the preloaded interfaces common to the four bolts was compromised. This newly designed shear feature ensured full shear capability and eliminated any risk of joint interface slippage. This design feature allowed for easy integration and avoided a high risk and precise match drilling operation on the major top deck component. This was a good reminder of a design engineering principle to value design for assembly. The interface between the CDPR and the mobility differential utilized the same match drilled shear pins and interface as MSL's design due to mobility differential remaining nearly heritage from MSL. Despite this particular interface still being match drilled, the re-designed shear boss feature of chassis bracket to top deck interface still required less time and effort.

Flexure Conceptualization and Trade-off for Mars 2020

As with MSL, the structural and compliant aspect for the Mars 2020 CDPR mechanism was to create a theoretical torsion spring about the CDP [1]. Unique for the Mars 2020 CPDR was to accomplish this with a lower torsional spring stiffness and overall assembly mass instead. As determined by simulation of EDL sequence in ADAMS, a reduced torsional stiffness about the CDP coupled with a reduced CDPR mass would linearly reduce the peak flight loads transferred into the rover chassis and mobility system. This finding was set forth as the design objective for the Mars 2020 CDPR where MSL's torsional stiffness of 200,000 N-m/rad [1] was halved to 100,000 N-m/rad to become the new Mars 2020 design parameter for the CDPR.

The reduction in effective torsional stiffness and mass reduction did come with a trade-off, however. The linear spring of the CDPR would be less stiff, yet still had the same amount of time to dampen out the resultant load at the center of the differential. While the load to dampen out from an asymmetric deployment would start-off lower, the more compliant linear spring would not be able to dampen out as much load as the MSL CDPR. This resulted in a higher load at the time of pin-puller firing for the Mars 2020 compared to MSL. From worst case ADAMS models with the softer Mars 2020 restraint system, the peak load (torque about the CDP axis or rover z-axis as denoted by "Mz") at the time of release was roughly 56% higher, but still within the capability of the pin-puller (Fig. 3).

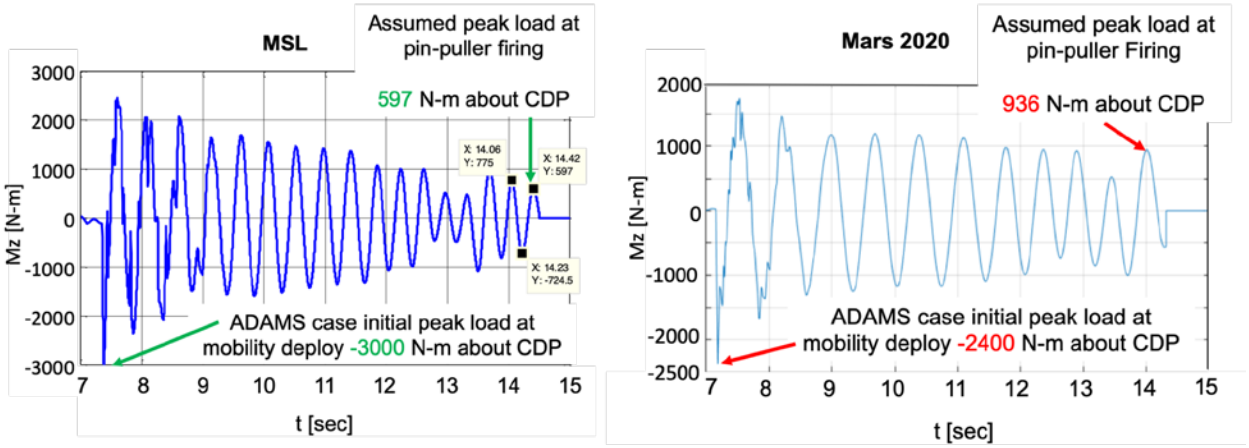

Figure 3. Moment about CDP of MSL vs. Mars 2020 showing the maximum torque through the CDP at the time of CDPR pin-puller firing: (a) MSL loads showing an initial higher peak mobility deployment load and a lower pin-puller firing load, (b) Mars 2020 loads showing an initial lower peak mobility deployment load and a higher pin-puller firing load.

Flexure Design and Development

With the target torsional stiffness about the CDP set, the design and placement of the spring-like flexure that would act as the damper for the CDPR was the first component of the CDPR to be fully prototyped and tested. The flexure design began with a simple cantilever beam concept. The multi-looped feature was then implemented and modeled by placing several cantilever beams in series to form a linear spring. In the early design phase, a MATLAB optimization program was created to determine the placement and sizing of the flexure in order to minimize mass while also achieving the target equivalent torsional stiffness about the CDP. A structurally optimum and mass efficient location of the flexure was determined to be the same as that of MSL; having the pin-puller attaching to the flexure 180.5 mm aft of the CDP axis. After this optimization determining rough sizing of flexure dimensions, the design transitioned to higher fidelity Finite Element Analysis (FEA) modeling to close in on a more final design of the flexure.

There were challenges in the initial design of the flexure to strike a balance between required material strength and structural buckling margin as well as target flexure compliance. To begin, Maraging 300 steel was selected as candidate material for the flexure due to its superior strength properties and high strength vs. stiffness ratio as material strength was the first design constraint to satisfy followed by structural compliance. To arrive to the first prototype design, extensive analytical iterations via FEA were performed in order to meet a rather narrow design window of stress, buckling, and stiffness requirements. Findings from the structural analysis indicated that peak stress magnitudes and distribution as well as overall flexure stiffness are highly sensitive to the width of the flexure loops followed by stem of the loops (Fig. 6).

Prior to Detailed Design Review (DDR), a flexure prototype out of the flight material specification and same lot of flight material was subjected to a series of structural characterization testing. Objectives of this testing was to statically characterize the flexure's uniaxial tension and compression stiffness at room temperature and qualification level hot (+40°C) and cold (-55°C) temperature up to CDPR's flight limit load (FLL). A final test would be conducted to determine the flexure's tensile residual strength capability at room temperature.

Since flexure strength and stiffness were two self-competing design constraints and overall CDPR compliancy in mobility deployment load absorption is entirely depending on the flexure stiffness, its physical measurement would serve invaluable to confirm FEA predictions. Fig. 4 shows the images of the nominal test set-up as well as deformed shapes under both tension and compression.

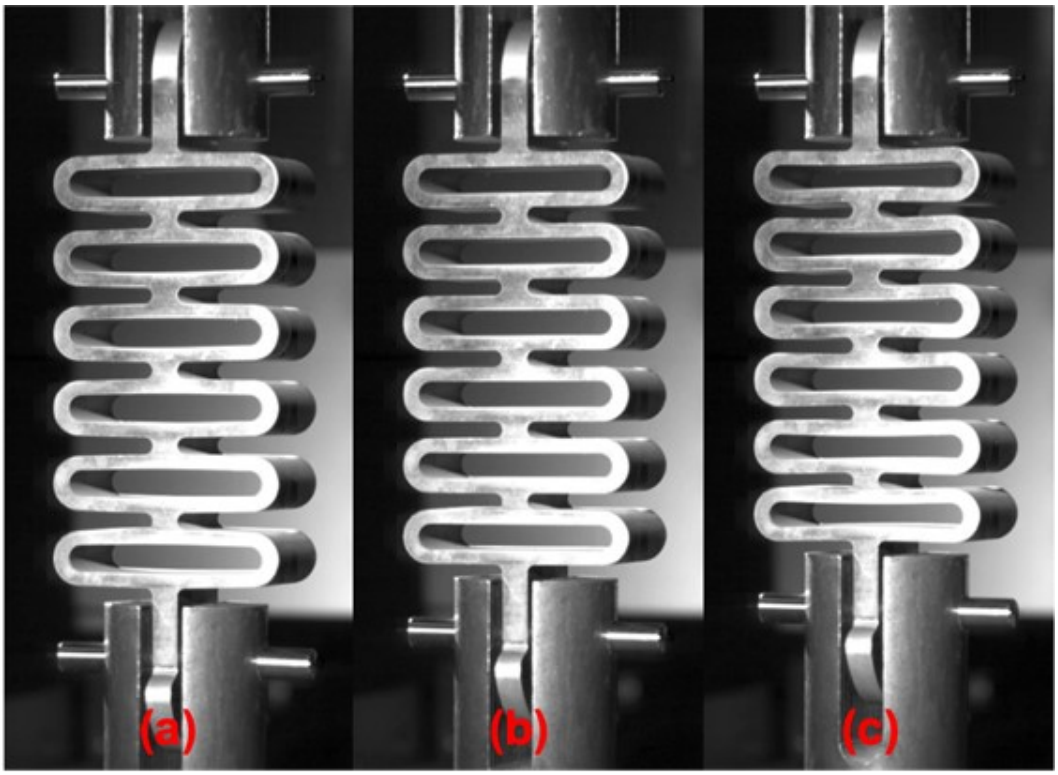

Figure 4. Fully reversed range of deflection of the prototype flexure at (a) max extension from tensile load, (b) nominal unloaded state, and (c) max compression from compressive load.

Below are the key findings from this flexure prototype characterization test:

- Flexure's uniaxial stiffness (load vs. deflection) appeared highly linear and repeatable at both room (illustrated in Fig. 5), hot, and cold temperatures with little to no signs of hysteresis over a set of 34 tension-compression cycles
- Temperature effects are minimal – within a maximum difference of 2% of the measured flexure's stiffness relative to the desired target stiffness
- Residual strength test achieved a tension load of approximately 46 kN, which demonstrated a 33% more tension load capability than predicted by linear FEA
- No signs of material yielding observed throughout the entirety of the test

This prototype testing sufficiently demonstrated that flexure critical stress concentrations exhibited more-than-adequate strength capability. Based on this, nonlinearity in material's elastic-plastic behavior as well as large displacement theory were incorporated in the FEA. This updated the predicted onset of yielding in the flexure to be approximately 71 kN, which was more than twice the initial predicted ultimate failure load, and 40% higher than the max load reached during the residual strength characterization test. This warranted the final round of flexure thinning to further reduce its stiffness and mass (Fig. 6).

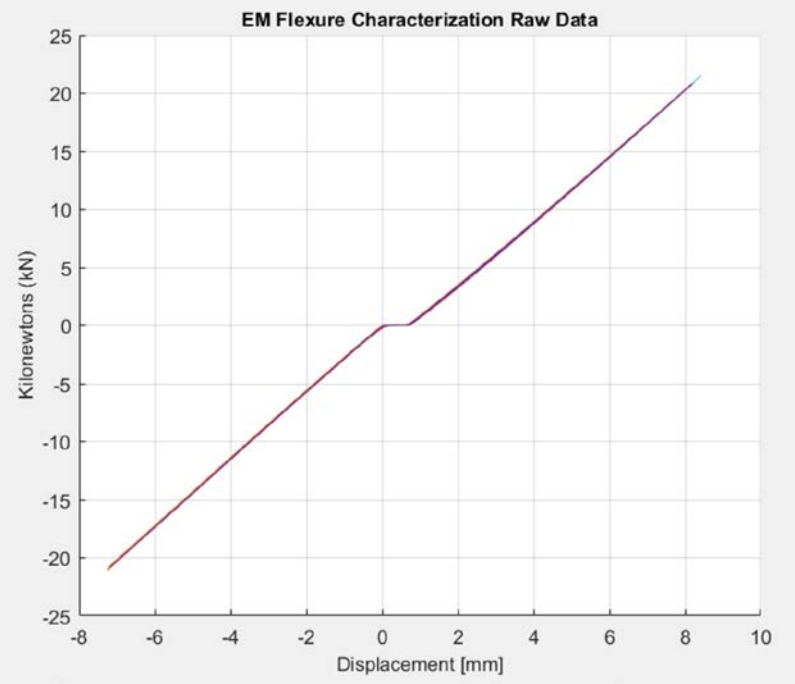

Figure 5. 15 overlaid cycles of raw force vs. displacement data at room temperature.

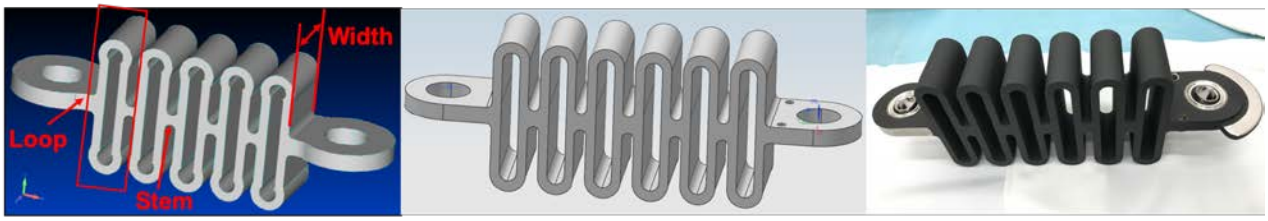

Figure 6. The evolution of the flexure design: (a) pre-Initial Design Review design, (b) proposed Detailed Design Review design, and (c) final delivered flight design.

The trade-off being after this final round of flexure thinning out, was that the flexure's lowest structural margin became buckling critical rather than based on local stress concentrations. Buckling test of the flexure was subsequentially performed post-DDR on a flight like design. Test results indicated no signs of structural buckling up to the required 1.4 test factor over the FLL presented at DDR. Resulting from this flexure developmental design and testing, the final design was proposed at DDR and was hardly changed for the final delivered flight flexure configuration post-DDR.

Deployment Mechanism

This new architecture of combining the compliant component (the flexure) and the deployable resulted in a redesign of the elements of the mechanism to deploy the flexure. More often than not, it required increasing size as well as strength of these elements. While the Mars 2020 CDPR had more components, the different approach of the mechanism resulted in approximately 50% less mass for the whole assembly while actuating a 10 times more massive deployable. The MSL deployment mechanism used symmetrical torsion spring to deploy a 150-gram linkage. The Mars 2020 deploys the 1500-gram flexure using larger asymmetric torsion springs, initial motion kickoff spring, and a magnetic latching hardstop to contain it in its deployed state. This section details the development of these elements of mechanism in the Mars 2020 CDPR as well as several findings and key lessons learned throughout the development process.

Torsion Springs

The main components to deploy the flexure are the torsions springs. At the time of DDR, it was required to show by design twice the needed torque to deploy the flexure to overcome mechanism frictional losses in dynamic environments. For Mars 2020, each torsion spring increased in size and strength compared to the MSL CDPR torsion springs. These larger torsion springs led to a design challenge of how to positively capture the two free ends of these larger torsion springs. For MSL, the torsion spring ends were manually bent to route the spring wire end through a hole in the titanium linkage. For larger Mars 2020 torsion springs, the spring wire was fabricated out of a stronger stainless-steel material and from spring wire nearly twice the diameter. There was concern if one could manually bend the spring wire accurately and without damaging the spring wire. Thus, it was chosen to have the vendor make the torsion spring with prescribed bends at each end.

The style of bends at the end of the torsion spring to route through the flexure was inspired from linkage rods found in automotive engines. There are two 90° bends at one end of the torsion spring and are routed through a hole in flexure. Then once the torsion spring is installed on its arbor, each torsion spring would be positively captured. The size and position of the pass-through holes in the flexure and the torsion spring bends were designed together to achieve this positive retention of torsion spring end in the flexure. In the end, this design proved to be easy to implement and less susceptible to damaging the hardware with a manual bending process. See Fig. 7 for photos of wire end bends of each torsion spring.

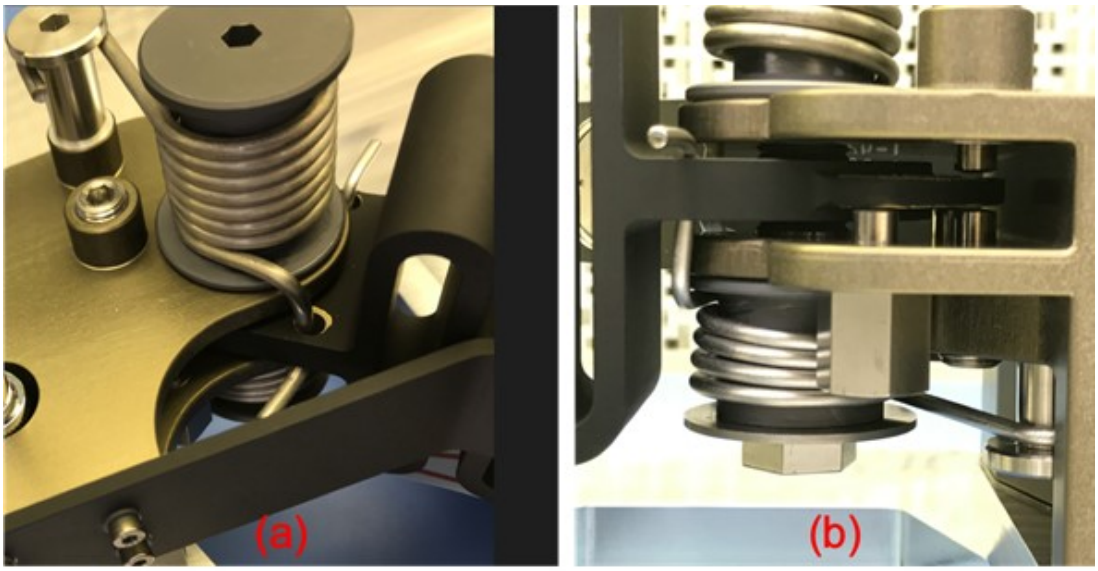

Figure 7. Views of torsion spring ends: (a) upper torsion spring, (b) lower torsion spring and the travel limiters are protruding through the chassis bracket clevis with set gaps to the back shelf on the flexure.

There were design space limitations on the lower of the two torsion springs, which resulted in an asymmetrical design. As a torsion spring is preloaded, the effective spring diameter is decreased and the overall spring length is increased. The lower torsion spring had a fixed height from the confined space between the chassis bracket bottom and top deck. There was concern that the lower torsion spring could get too long when the flexure is in its stowed state. The upper torsion spring did not have the same height limitations and could have more loops and delivery more torque for the same deflection. The combination of the two asymmetric springs surpassed the DDR requirement of 100% torque margin, roughly 66% of the combined delivered torque came from the upper torsion spring. However, the fault case of only the lower torsion spring acting was enough still to deploy the flexure. To verify this release redundancy capability, various prototype and Dynamic Test Model (DTM) tests have indeed demonstrated that the mechanism could still deploy fully without the upper, stronger, torsion spring contributing to the deployment.

Initial Motion Kickoff Spring

To adhere to flight mechanism design principles, a kickoff spring to aid in the initial deployment of the flexure was required to be added after DDR. This leaf spring, also made out of corrosion resistant steel (CRES), was placed within the clevis gap of the CDPR's bracket connected to the aft of the differential, the Horizontal Swing Arm (HSA) bracket. With its preload, the spring was designed to exert a force on the flexure lug to minimally displace the flexure approximately 9.5 mm, or the diameter of the pin-puller pin. Prototype testing yielded two findings: first that the leaf spring did not need conditioning, but that the end interfacing with the flexure was digging into the paint of the flexure and causing the paint to shed. Two actions were taken from this lesson learned: (1) incorporate a slight curvature on the kickoff spring end contacting the flexure for a smooth point of contact, and (2) mask the potential contact area of the kickoff spring and flexure lug side to avoid any flexure paint scraping. Lastly, a coating of dry-film lubricate was applied to minimize friction of the contact surface on the kickoff spring. See Fig. 8 for the kickoff spring configuration with the flexure in the stowed position.

The addition of this spring had several benefits for designing a flight mechanism. Not only did it add extra deployment force for the mechanism, but also fail-safe capability in a fault case to ensure the mechanism functions as intended if the larger and more capable upper torsion spring functionally or structurally fails. This more robust fault case configuration significantly boosted confidence that the CDPR will work as required for the critical separation prior to touchdown on the Martian surface. All these benefits are an important lesson learned of why it is flight design principle to have an initial motion spring for a deployable.

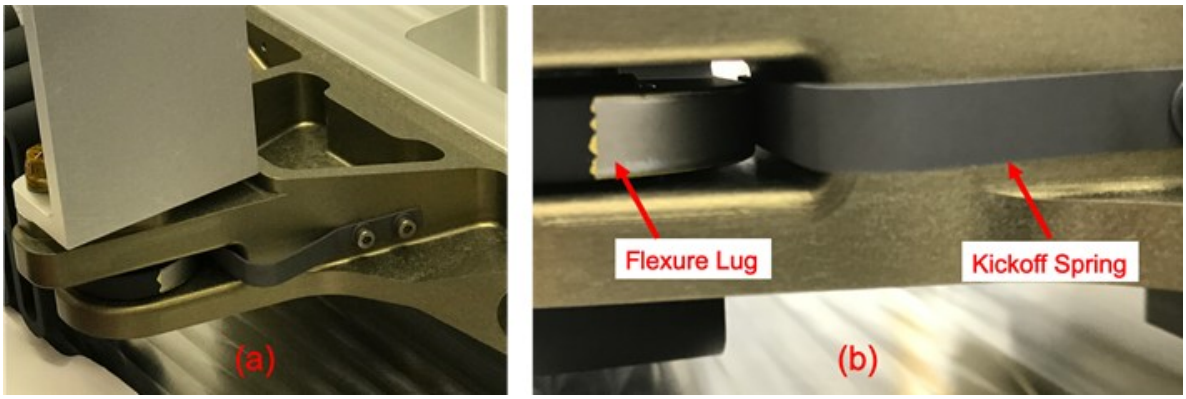

Figure 8. Views of initial kickoff spring: (a) view of kickoff spring attached to the HSA bracket, (b) view inside the bracket clevis where the spring interfaces with the bare flexure lug.

Travel Limiters

With the new Mars 2020 design, the larger height and length of the flexure as well as the rotational degrees of freedom in the spherical bearings at two ends of the flexure introduced a few close clearance concerns in the mechanism. At nominal (when flexure is engaged or not yet released), the 10.3 mm vertical clearance between the chassis top deck and flexure was found insufficient in the event if the flexure pitches downward when it exits out of the HSA bracket during deployment. During testing without the torsional springs, there was a roll rotational degree of freedom in the flexure, which allowed flexure contact with the chassis bracket due to residual rotations from the spherical bearings at two ends of the flexure.

To address these concerns of interference, features on the chassis bracket were implemented to adapt four (4) vertical travel limiters at the clevis region of the chassis bracket. Two of them are opposite of and vertically aligned with each other with one above and below the flexure lug that control the vertical up-and-down pitch. The remaining two are located at two sides of the center lower limiter and are designed to control the roll of the flexure. These travel limiters are fabricated out of Nitronic 60 for material compliancy and high surface wear capability and are designed in pin-like shapes with spherical tips, which were also coated with dry-film lubricant. A back fin extrusion on the flexure end lug common to the chassis bracket was added as contact region for the travel limiters. See Fig. 7 for configuration of its design.

It was another lesson learned about the contribution of torsion spring preload to the flexure's pitch and roll angles. The flexure to chassis bracket contact from flexure roll was found after DDR with the chassis bracket already fabricated. Therefore, it was a considerable challenge to accommodate the additional roll limiters at this stage of hardware development. When having larger springs attach to hardware with degrees of freedom, the influence on the hardware's orientation from spring preload should be accounted for.

Magnetic Hardstop

Similar to how the kickoff spring added additional fail-safe margin and a fault case to the deployment, the magnetic latching hardstop had similar additional benefits for the final deployed position. Due to the larger flexure deployable, there was close clearance concern to the surrounding hardware after deployment, namely the aft bridle tower and its surrounding harnessing on the chassis top deck. A final deployment angle of 40° was chosen to split the difference between the minimum rotation needed by the flexure to clear the range of motion of the differential and aft bridle tower.

From initial testing, there was concern that with the initial hardstop design induced a substantial amount of flexure rebound due to its stiff nature stemming from a C-channel profile design. After initial contact with the hardstop, the flexure would then require three re-contacts with the hardstop to come to a complete rest. Around the DDR, the hardstop went through two major redesigns. First, the structural shape was made to be a standard aluminum sheet metal profile. The final design was the same sheet profile with a bore feature added to house the magnet and its casing (Fig. 9). This diving-board like design added significant compliancy such that the hardstop would dampen out the initial contact of the flexure and reduced the amount of flexure rebound after initial contact. However, during developmental tests, this elastically compliant hardstop rotated nearly 8° over the planned 40° rotational travel for the final deployed position. This exceedance approached the close clearance to the aft bridle tower but did not violate the clearance margin. It was deemed acceptable after being closely monitored at flight level functional testing.

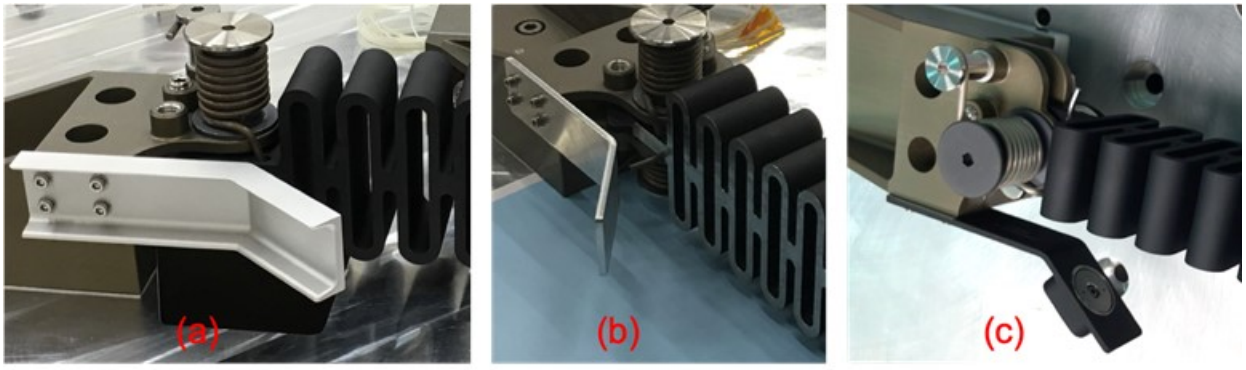

Figure 9. Development of the hardstop: (a) initial stiffer C-channel profile, (b) DDR sheet metal design, (c) thinner profile with a feature to house the magnet in the final magnetic hardstop.

As a second function, the hardstop is to restrain the deployed flexure once it's deployed such that the rover differential is completely free to rotate. This hardstop design utilized the flexure's Maraging 300 steel magnetic properties to make a magnetic latch. The magnetic force of this latch would be added to the residual capability of the torsion springs. The magnet to be used is of the same material as other magnets on Mars 2020, Grade N42 Neodymium. There was concern about the likelihood of magnet fracture due to its brittle nature directly from impact of the flexure to hardstop contact. To address this, a protective stainless-steel housing was incorporated. For securement, a ring magnet design was chosen to allow a fastener to run through the magnet and housing and the magnet was to be potted inside the assembled housing (Fig. 10).

Several lessons were learned in the prototyping of the magnet housing. The magnet housing is two separate pieces that when mated together there is a void that would fit the ring magnet. To have the

magnetic latch work, a magnetic flux circuit with the magnet housing and flexure needs to be closed. Most flight acceptable CRES are austenitic, with the exception of 400 series CRES, which is a ferritic CRES. It was learned that the part of the housing in contact with the magnet should also be the part that is closest to the flexure when the flexure is in contact to the hardstop. This piece of the housing should also be a ferritic steel to complete the magnetic flux circuit from the magnet, through the ferritic housing component, through the flexure, and return to the magnet (Fig. 10). This is what produced the latching force. The top of the magnet housing should be an austenitic CRES. Otherwise, the magnetic flux would short through the top part of the magnet housing and not through the flexure. The final design called out the back part of the magnet housing to be 410 CRES and the top part to be 303 CRES. This allowed the magnetic latching force to flow from the magnet through the flexure. The delivered magnetic holding force for the flight unit was measured to be an average of 24.4 N.

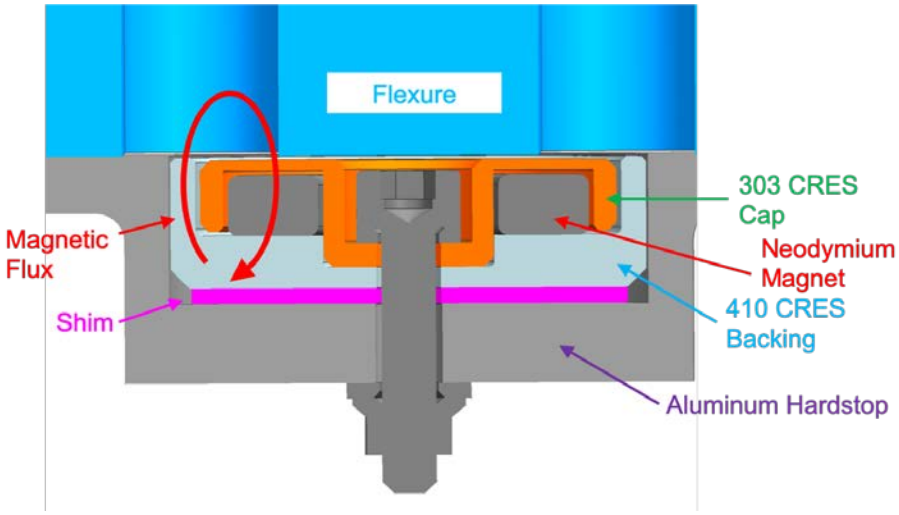

Figure 10. Cross section of the magnet in its CRES housing with the flexure against the hardstop. Also showing the magnetic flux circuit, which produces the holding force of the magnetic latch.

There was a lesson learned that while magnetic latches could be used, some permanent magnet materials cannot tolerate higher temperatures. To comply with mission planetary protection requirements, this neodymium magnet would have seen temperatures during vacuum bakeout such that the magnet could have lost some of its residual magnetic strength. As a result, the magnet and its housing were excluded from vacuum bakeout as well as parts of other non-functional tests that went over +80°C. Planetary protection requirements were satisfied with other methods rather than a vacuum bakeout. In future magnetic latches, it is recommended that the magnet can withstand higher temperatures without any risk of losing magnetic strength over the whole non-operational temperature range.

CDPR Design Validation and Verification (V&V) Testing

Since the Mars 2020 CDPR was non-MSL heritage, this new assembly was subjected to a full design V&V campaign that involved a series of functional and structural testing at various level of build integration. As of January 2020, all testing was completed. Rather than presenting the entirety of this lengthy test campaign, two (2) significant tests and some key lessons learned are highlighted. For a complete summary of the test programs in order of execution (including the prototype testing during the engineering development phase), see Table 1 and Table 2 at the end of this section.

Engineering Model (EM) “Dirty” Testing

When the CDPR mechanism is fully actuating, in the power decent stage of EDL, there is a lot of Martian regolith that could get kicked up and lodged into the numerous controlled gaps within the mechanism. This raised a concern that the deployment of the flexure could be hindered by this “dirty” condition. To address

this concern, “dirty” testing was performed as a dynamic functional test to ensure its full deployment capability in such an environment. The “dirty” environment was simulated via a media mixture designed to simulate Martian regolith being blown into the CDPR. Using nitrogen gas (GN_2), 700 ml of this media was distributed throughout the entire mechanism and around the mechanism revolute joints. After 30 seconds of circulating the media and thoroughly coating the mechanism, a cord connected to a manual pin (to replace the pin-puller) was pulled to deploy the mechanism.

This functional test completed successfully by demonstrating full deployment capability under such “dirty” condition with no signs of hindering. This testing was performed prior to the development of the kickoff spring. This showing that only the redundant torsion springs were sufficient to deploy the flexure and the added kickoff spring only added margin on top of this. To further demonstrate the robustness of the mechanism, a worst-case scenario was also tested where the redundancy of the torsion springs was eliminated and flexure deployment under the “dirty” condition was only driven by the lower and smaller torsion spring. With that, the CDPR still deployed its flexure successfully with no signs of any hindering. See Fig. 11 for photos of the test configuration.

Figure 11. Showing the “dirty” test configuration: (a) showing the before the mechanism was coated with the Mars regolith simulate media, (b) after media circulation and deployment. This test was for the fault case with only the lower torsion spring having successfully deployed the flexure.

Engineering Model Loaded Deployment Testing

From the rover descent simulation in ADAMS, it was determined that the CDPR would sustain approximately 5.2 kN of residual load at the time just prior to pin-puller firing (Fig. 3). Such amount of residual load would result in approximately 5 joules of potential energy being stored within the fully restrained CDPR. At DDR, this led to a concern that once the pin-puller fires and the flexure becomes unpinned, the then “open” system of CDPR could have an unpredictable and undesirable dynamic response from the sudden release of the strain energy stored in the flexure. To address this, another dynamic functional test was conducted where the CDPR would be deployed while under 1.2x peak load (6.2 kN through the mechanism). This “loaded deployment” testing employed a flight-like configuration using a pneumatically driven pin-puller. All springs, magnetic hardstop, and travel limiters were present in this test and in a flight-like configuration. See Fig. 12 for loaded deployment test configuration.

Using a crane and load cell, a lateral load was applied to one side of a Ground Support Equipment (GSE) revolute joint to mock the differential CDP, this in turn induced an equivalent load through the CDPR in the opposite direction. A total of five tests were conducted with this setup. Since polarity of such residual load in flight is not 100% certain, the mechanism would be deployed under a tensile load and then a final

compression load through the CDPR for full coverage. From the tensile deployments, the mechanism performed nominally. From high-speed video footage, some elastic spring back of the flexure along its length from the release of tensile strain energy was observed. However, the flexure continued onto its deployment as driven by all the springs. This form of dynamic response was expected and deemed acceptable. During the deployments in compression, however, functional failures were encountered. The following section dives into the test failure observation, the respective actions carried out post-failure, as well as lessons learned.

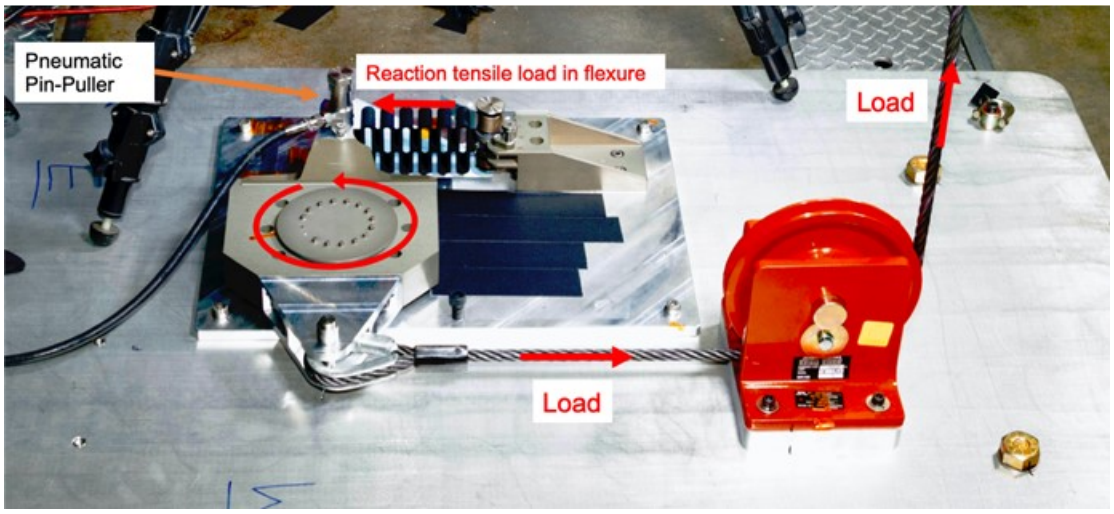

Figure 12. Loaded deployment tensile test configuration. The vertical load from the crane is reacted with a linear tensile load in the flexure. The pneumatic pin-puller fires when the crane is at the 1.2x peak load.

During this tensile portion of the loaded deployment testing, it was observed the GSE rotated very quickly about the mock CDP revolute joint due to the strain energy release in the test setup. This configuration resulted in the GSE rotating out of the way of the flexure deploy path; resulting in no interference in deployment. However, when flexure preload was reversed to compression, such GSE rotation after releasing the pin-puller was also reversed. As a result, this reversal caused the GSE to rotate towards the flexure path of deployment and subsequently jammed the flexure; leaving approximately half of the applied preload stored within the system. Once the load was relaxed to nearly zero, the flexure was able to fully deploy. Upon inspection of the hardware post-test, no damage was observed other than minor paint marring on the flexure. To fully ensure this anomaly was truly realistic and repeatable, this compression test was repeated for the final test and same jamming results occurred.

The cause of the mechanism jamming was determined to be a function of the test GSE. The GSE rotated two orders of magnitude faster than the fastest predicted flight CDP rotation rate from ADAMS. It is because of this non flight-like, extremely high rotational rate of the CDP, subsequent jamming occurred. More importantly, this jamming event showed that there was a race condition designed into the hardware.
This race condition was new and solely problematic for the Mars 2020 CDPR. The overall height of the flexure linkage was big enough to completely block a moving HSA bracket clevis if it does rotate towards the flexure. For MSL, the linkage was only as thick as the spherical bearings and therefore; not big enough to be in any vicinity of the rotational path of the HSA bracket if the linkage was stagnate.

To alleviate the concern of this race condition, a simulation of the fault case CDPR deployment against the fastest ADAMS predicted rotating differential was visited. Using as-tested data from CDPR deployments, an analytical model was created that could output the position of the flexure at any point during its deployment. For best accuracy, all environmental conditions such as temperature, orientation, and level of “dirtiness” were considered and properly verified from previous developmental tests. From this verified analytical model, the outputted flexure positions were compared against the worst-case differential position

from ADAMS models for the deployment. Results indicated that flexure contact would only occur if the worst-case initial differential offset and rotational rate are increased by a factor of 2.6 while the CDPR is in this fault case configuration. This was determined to be sufficient margin against extreme environmental cases that the CDPR would win the race condition.

Table 1 – EM prototype and developmental testing matrix in order of execution

Test Type	Test Objective(s)	Outcomes
EM Flexure Characterization	Characterize stiffness at operational/non-operational qualification temperatures and tensile residual strength of the first flexure prototype	Successful, no anomalies
EM Thermal Functional Testing	Demonstrate full deployment mechanism capability at operational/non-operational qualification temperatures in both nominal and fault configuration	Successful, no anomalies
EM Dirty Testing	Demonstrate full deployment mechanism capability while in a dirty environment from regolith kicked up during powered descent of EDL	Successful, no anomalies
Flight-like Flexure Characterization and Buckling	Characterize stiffness and buckling capability up to 1.20x and 1.40x FLL, respectively, at room temperature and respective operational temperatures.	Successful, no anomalies
Loaded Deployment Testing	Demonstrate full deployment mechanism capability under 1.20x FLL	Anomaly: jamming observed during compressively loaded deployment, identified race condition in CDPR deployment.
Magnet Thermal Testing	Characterize thermal effects on magnet installed in the hard stop	Successful, confirmed thermal concerns for neodymium

Table 2 – DTM and FM V&V test matrix in order of execution

Test Type	Test Objective(s)	Outcomes
DTM and FM Flexure Characterization	Characterize spring rate of DTM and FM Flexure to 1.2x and 1.0x FLL, respectively at operational/non-operational temperatures.	Successful, no anomalies
DTM and FM Vacuum Bakeout	Thermally eliminate contamination and outgas any volatiles prior to launch	Successful, no anomalies
DTM CDPR Random Vibration (assembly level)	Demonstrate structural capability against protoflight launch environment	Successful, no anomalies
DTM Thermal Functional Testing	Demonstrate full deployment mechanism capability at operational/non-operational qualification temperatures in both nominal and fault configuration	Successful, no anomalies
FM Thermal Functional Testing	Demonstrate full deployment mechanism capability at operational/non-operational hot/cold flight acceptance temperatures	Successful, no anomalies
FM CDPR Random Vibration (Power Decent Vehicle Level)	Demonstrate structural capability against protoflight launch environment	Successful, no anomalies
DTM Mobility Deploy	Demonstrate full dampening of the resultant load during rover asymmetric mobility deployment and full CDPR deployable functionality in earth gravity	Successful, no anomalies
DTM Rover Chassis and Differential Qualification Static Test	Structurally qualify the entirety of CDPR by demonstrating strength capability up required 1.20x FLL	Successful, no anomalies
DTM Rover Chassis and Differential Qualification Static Test – CDPR Deployment	Demonstrate full deployment mechanism capability under required 1.20x FLL	Successful, no anomalies

As a worthy note, through this race condition analysis of CDPR deployment fault case, the kickoff spring made the deployment time approximately 33% faster than if there was only the lower torsion spring available to drive the deployment. Such a finding reaffirmed that incorporating an initial motion spring (the kickoff leaf spring) is a great sound design principle.

This loaded deployment test was repeated in January 2020 as the last part of the DTM rover chassis and differential design qualification static testing campaign. The CDPR was loaded to 1.2x the limit loads in tension. The flexure was deployed in this configuration using a flight-like pin-puller. No jamming occurred and the same expected dynamics response of the flexure from the strain energy release was observed, resulting in a successful test.

Summary

For the Mars 2020 mission, a new CDPR achieved similar functionality as the MSL design, while using only half the mass for the structural mechanism by using a new mechanism architecture. The MSL crank-slider mechanism, which was sensitive to misalignment and structural concerns, was replaced with a two-force member spring-like flexure that doubled as providing compliance for the system and as the deployable. This flexure proved to have verified robust design. It was repeatable at temperature and did not require any conditioning.

However, this larger deployable required the torsion springs and other hardware of the mechanism to deploy the flexure to be increased in size and strength in order to actuate this larger deployable for the Mars 2020 CDPR. Having the flexure double as the spring dampener and the deployable had the benefit of eliminating the required alignment precision from the MSL CDPR, but also introduced new close clearances and race conditions. The biggest lesson learned was to not have race condition potential in a deployable mechanism. It was a large amount of engineering effort to properly show that the mechanism would win this race condition. The analysis on the race condition reaffirmed an important design principle, to always have a simple initial motion spring integrated into a deployable mechanism. Future mechanism could utilize the design of the CDPR flexure to create a tunable linear spring while ensuring the design does not have the same race condition concerns that were learned from.

Acknowledgements

This research was carried out at the Jet Propulsion Laboratory, California Institute of Technology, under a contract with the National Aeronautics and Space Administration. © 2020. California Institute of Technology. Government sponsorship acknowledged.

References

1. Jordan, E. 2012, Mars Science Laboratory Differential Restraint: The Devil is in the Details, Proceedings of the 41st Aerospace Mechanisms Symposium, Jet Propulsion Laboratory, May 16-18, 2012